

AutoQB: AutoML for Network Quantization and Binarization on Mobile Devices

Qian Lou Lantao Liu Minje Kim Lei Jiang
 Indiana University Bloomington
 louqian@iu.edu lantao@iu.edu minje@indiana.edu jiang60@iu.edu

Abstract

In this paper, we propose a hierarchical deep reinforcement learning (DRL)-based AutoML framework, AutoQB, to automatically explore the design space of channel-level network quantization and binarization for hardware-friendly deep learning on mobile devices. Compared to prior DDPG-based quantization techniques, on the various CNN models, AutoQB automatically achieves the same inference accuracy by $\sim 79\%$ less computing overhead, or improves the inference accuracy by $\sim 2\%$ with the same computing cost.

1. Introduction

Though convolutional neural networks (CNNs) have been the dominant approach to solving a wide variety of problems such as natural language processing, recommendation systems and computer vision [14], it is very challenging for mobile devices having limited hardware resources and tight power budgets to adopt CNNs, because of their large essential computing overhead, e.g., an AlexNet [14] inference involves 6 million weights and 1.5 billion floating point operations. A flurry of network acceleration techniques have been proposed to improve the computing efficiency of CNNs by network quantization [18, 10] and binarization [29, 36]. Network quantization transforms floating point weights and activations to lower precision n -bit fixed-point values, and computes inferences by cheap fixed-point multiply-accumulate (MAC) operations, where n is the *quantization bit number* (QBN). Binarization converts each weight and activation into m -bit binary codes $\{-1, +1\}$, and performs inferences by hardware-friendly binary logic operations, i.e., XNORs and population counts (popcounts), where m is the *binarization bit number* (BBN). Network quantization and binarization enable the deployment of CNNs on mobile devices by significantly decreasing the inference computing overhead.

How to decide the QBN (BBN) is the most important task of network quantization (binarization). The hand-crafted heuristics required by deciding QBN (BBN) influencing the inference accuracy, computing latency and overhead are so

sophisticated that even machine learning experts usually obtain only sub-optimal results. Recent works [32, 5] automatically select a QBN for each layer of a CNN through a DDPG [15] or LSTM-based reinforcement learning (RL) framework without human intervention. However, it is still difficult for small mobile devices such as drones, self-driving cars and Google glasses, to adopt such *course-grained* quantized network models using a QBN for each layer, because their limited battery lifetime makes them sensitive to the bit-width of MAC operations and memory accesses during inferences. Although previous works [9, 17] suggest different weight output channels in a layer have different amounts of redundancy and thus various impacts on inference accuracy, to the best of our knowledge, no prior work sets a QBN for each weight output channel in a CNN layer, because of the huge design space. For example, the 5 CNN layers of AlexNet have 688 weight output channels. If each output channel has a QBN ranging from 1 bit to 32 bits, we need to pick up the configuration achieving the best inference accuracy by the smallest QBNs among 32^{688} combinations.

As CNN architectures are advancing fast and becoming much deeper, it is infeasible to employ rule-based domain expertise or even conventional RL-based techniques to explore the exponentially enlarging channel level *fine-grained* network quantization/binarization design space, particularly when considering both weights and activations. Therefore, we propose AutoQB that leverages hierarchical DRL to automatically search the weight (activation) output (input) channel level design space to improve the quality of network quantization/binarization. AutoQB relies on a hierarchical DRL agent [20, 21] consisting of a high-level controller (HLC) and a low-level controller (LLC). The HLC learns to set an average QBN/BBN for a layer as a *goal*, while the LLC learns how to quantize/binarize weights (activations) of each output (input) channel to meet its goal. Two controllers in the hierarchical DRL agent simultaneously learn by trials and errors, i.e., penalizing inference accuracy loss while rewarding smaller QBNs/BBNs.

2. Background and Related Work

Network Quantization. Instead of 32-bit IEEE754 floating point operations, previous works [38, 10, 3, 18, 8, 16]

accurately train a CNN by 16-bit fixed point parameters and perform accurate inference by ≤ 8 -bit fixed point arithmetic operations. For an uniform quantizer [16], the range of a fixed point number approximately equals to $resv \cdot 2^{QBN}$, where $resv$ is the resolution. Compared to an uniform quantizer [16], dynamic fixed point [3] and logarithmic quantizer [19] fit the non-uniform weight distribution better. As Figure 1(a) shows, quantized CNNs perform inferences by fixed point binary multipliers and adders. Inside a binary multiplier, a quantized weight and a quantized activation do AND operations bit by bit to generate intermediate results that will be accumulated (ADD) by binary adders.

Network Binarization. To further reduce inference computing overhead, previous works binarize CNN weights [13, 36, 7, 29] and activations [24, 17, 39] into multi-bit binary codes $\{-1, +1\}$. As Figure 1(b) exhibits, binarized CNN inferences rely on bit-wise logic operations, i.e., XNORs and popcounts, rather than floating point MACs. To binarize a network layer, the real-value weight filter $W \in \mathbb{R}^{w \times h \times c_{in} \times c_{out}}$ is estimated using the linear combination of BBN_w binary filters $B_1, \dots, B_{BBN_w} \in \{-1, +1\}^{w \times h \times c_{in} \times c_{out}}$ [17] such that $W \approx \alpha_1 B_1 + \alpha_2 B_2 + \dots + \alpha_{BBN_w} B_{BBN_w}$. The real-value activation A can be binarized to the linear combination of BBN_a binary activations A_1, \dots, A_{BBN_a} in a similar way [17]. Therefore, we can have $Conv(W, R) \approx \sum_{m=1}^{BBN_w} \sum_{n=1}^{BBN_a} \alpha_m \beta_n XNOR(B_m, A_n)$.

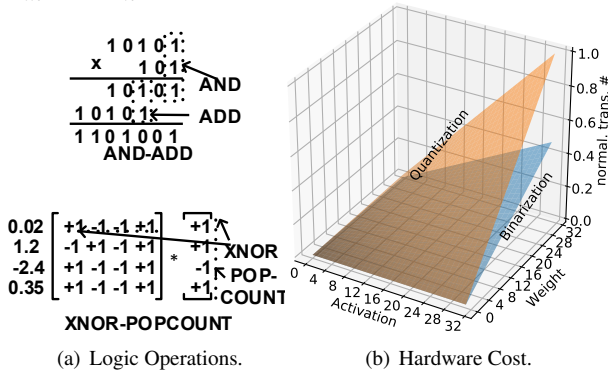


Figure 1: The Comparison Between Network Quantization and Binarization (All hardware costs are normalized to that of floating point MAC units).

Hardware Cost. Quantized CNNs need only cheap fixed-point MAC units, while binarized CNNs rely on massive XNOR gates, low cost popcount units [23], and few fixed-point multipliers. The hardware cost comparison between network quantization and binarization is described in Figure 1(b), where we show the $(32nm)$ transistor number of the logic units that can finish the convolutions of a quantized/binarized output channel in a cycle ($100MHz$). All data in the figure is normalized to the hardware overhead of a full precision model with 32-bit floating point weights and activations. With a decreasing QBN (BBN) on weights or/and activations, the hardware cost of a quantized (bina-

alized) CNN is significantly reduced. Compared to a quantized CNN, its binarized counterpart with the same weight and activation bit-widths consumes much less transistors.

Table 1: The comparison of RL-based techniques for network design space exploration.

Features	N2N[1]	ReL[5]	AMC[9]	HAQ[32]	AutoQB
hierarchical deep RL	X	X	X	X	✓
search for quant. & binar.	X	X	X	X	✓
channel level exploration	X	X	X	X	✓
search for act. and weight	X	X	X	✓	✓
fast non-RNN agent	X	X	✓	✓	✓

AutoML and Network Design Space Exploration. Recent works take advantage of reinforcement learning (RL) [2, 40], genetic algorithm [28, 26] and Bayesian Optimization [12, 27] to automatically architect deep CNNs for higher inference accuracy. N2N [1] uses network transformation and RL to explore the design space of network compression. The weight channel pruning is automatically conducted by deep RL [9] and genetic algorithm [33]. ReLeQ [5] quantizes only weights for each layer of a CNN by LSTM-based RL, while HAQ [32] selects a QBN for each layer through a DDGP-based RL framework. Table 1 compares AutoQB against prior RL-based network transformation, compression and quantization techniques. Compared to prior works, AutoQB is the **first** work to automatically perform channel level quantization and binarization on both weights and activations of a pre-trained CNN model for mobile devices by hierarchical deep RL [20, 21].

3. AutoQB

By a recent off-policy hierarchical deep RL framework, HIRO [20, 21], we build AutoQB described in Figure 2. To quantize/binarize weights (activations), a weight output (activation input) channel $OC_i (IN_i)$ in a convolutional and fully-connected layer L_t , the AutoQB agent receives an observation s_i encoding necessary characteristics of the layer, where i is the index of weight output and activation input channels in the network; t is the index of all convolutional and fully-connected layers in the network. It uses its high-level controller (HLC) generates a weight goal gw_t , the average QBN/BBN for all weights of the layer, and an activation goal ga_t , the average QBN/BBN for all activations of the layer. Based on $gw_t (ga_t)$ and s_i , a low-level controller (LLC) of AutoQB generates an action $aw_i (aa_i)$, each of which is a QBN/BBN for all weights (activation) of each output (input) channel $OC_i (IC_i)$. The goal $gw_t (ga_t)$ remains for the next $c_{out} (c_{in})$ steps until the weights of all c_{out} weight output (c_{in} activation input) channels of the layer are quantized/binarized, where $c_{out} (c_{in})$ is the output (input) channel number of the layer L_t . After the LLC sends an action to the environment, the AutoQB agent receives an *extrinsic* reward (R_i) from the environment, and aims to maximize the cumulative extrinsic reward. The HLC is responsible for evaluating how well a goal has been accomplished and provides an *intrinsic* reward r_i to the LLC which

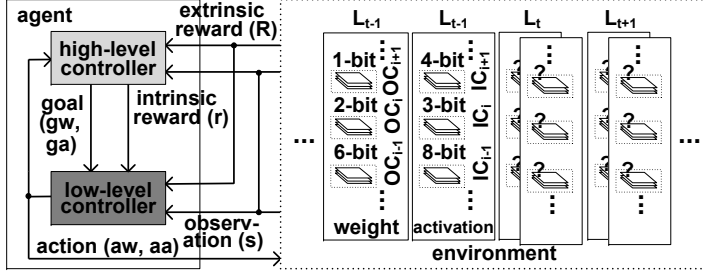


Figure 2: The overview of AutoQB.

focuses on maximizing cumulative intrinsic reward.

AutoQB supports a universal search protocol by using NetScore [35] that is a metric assessing the balance between inference accuracy, computing overhead, and architectural complexity of a network. By adjusting the parameters of NetScore integrated in the reward function of AutoQB, for a CNN model, AutoQB can search the best inference accuracy given the maximum amount of hardware resources; or the fastest and smallest model without inference accuracy loss. Instead of using a direct feedback [32] from heavy and slow hardware simulators, AutoQB adopts a lightweight Roofline model [34] to take the latency and energy of a specific hardware platform into consideration. Through the Roofline model, AutoQB captures approximately linear relationships between network parameters and hardware metrics by fitting parameters. For example, a larger number of logic operations indicates longer inference latency, while smaller QBNs/BBs for network parameters mean less memory accesses. These fitting parameters can be plugged into NetScore to estimate the hardware inference latency and energy in the AutoQB extrinsic reward. To accelerate the calculation of extrinsic rewards, the validation accuracy of the quantized/binarized network is evaluated without fine-tuning, which is an effective delegate of the fine-tuned accuracy [9]. After the network quantization and binarization policy search is done, the best-explored model is fine-tuned to obtain the best inference accuracy.

3.1. Problem Definition

AutoQB automatically quantizes/binarizes each output/input channel characterized by inputs, weights, and activations in a CNN layer. It uses a linear quantization strategy [38] to convert floating point output channels to fixed-point representations. Or it relies on a simple binarization technique [17] to transform each input, weight and activation to multi-bit binary codes $\{-1, +1\}$. Other more advanced quantization and binarization can be easily integrated into AutoQB to further improve the quality of quantized/binarized network without modifications.

Our goal is to precisely find a QBN or BBN for each weight output or activation input channel in a network to maximize the accumulative (extrinsic) reward defined by users. However, such channel level QBN/BBN search is never manually done before due to its huge design space. In

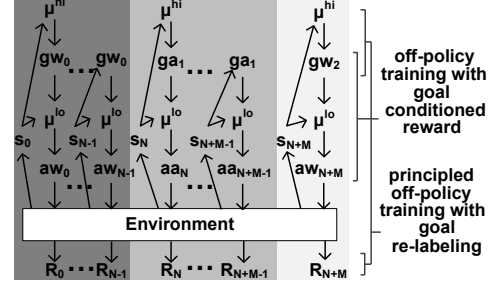


Figure 3: The working flow of AutoQB.

this paper, we train a hierarchical DRL framework, AutoQB, to automatically quantize/binarize a CNN with minimal inference accuracy loss.

3.2. Quant/Binarization with Hierarchical DRL

AutoQB adopts the hierarchical DRL HIRO [20, 21] for efficient search over action space. We introduce the detailed setting of AutoQB as follows.

State Space. For each layer L_t , to characterize a state (observation) s_t , we have following items:

$$s_t = (i, t, c_{in}, c_{out}, w, h, str, k, logic_t, rdc, rst, gw_t, ga_t, aw_i, aa_i, wvar_i) \quad (1)$$

where i is the index of weight output and activation input channels in the network; t is the index of convolutional and fully-connected layers in the network; the weight kernel shape is $c_{out} \times c_{in} \times k \times k$; and the input dimension is $c_{in} \times w \times h$. str is the convolution stride size. $logic_t$ indicates the XNOR number of layer L_t for network binarization or the number of AND operations [6] happening between each bit of two fixed point operands in layer L_t for network quantization. Compared to the 32-bit full precision network, rdc is the total number of reduced logic operations in previous channels. rst represents the number of remaining logic operations in the following channels. gw_t is the goal for weights, while ga_t is the goal for activations. aw_i is the action for the weight output channel OC_i , and aa_i is the action for the activation input channel IN_i . $wvar_i$ is the weight variance of OC_i . To reduce the activation action search space, AutoQB set the same QBN/BBN to all activation input channels in a fully-connected layer.

Goal and Action Space. The HLC produces an average QBN/BBN for weights or activations of each layer as a goal, while the LLC generates a QBN/BBN for each weight output or activation input channel in a layer as an action. A goal can be any real value between 0 and 32, while an action has to be an integer between 0 and 32. 0-bit indicates a layer or an output channel is pruned. The hierarchical DRL framework [20, 21] of AutoQB depends on a variant of DDPG, so it can provide a continuous space for goals and actions. A prediction result from the LLC is round to the closest integer to serve as an action. To accelerate the search, AutoQB limits the low-level weight action search space and enforces $\forall x, y \leq c_{out} \wedge x \neq y, (\frac{aw_x}{aw_y} - 1)(\frac{wvar_x}{wvar_y} - 1) > 0$.

Hierarchical DRL Agent. AutoQB uses a hierarchical DRL off-policy actor-critic agent [20, 21]. As Figure 3 shows, the HLC trains a deterministic neural network policy μ_ϕ^{hi} with its state-action Q-function Q_θ^{hi} by performing gradient updates on parameter sets ϕ and θ . The Q-function is trained to minimize the average Bellman error through $\varepsilon(s_i, a_i, s_{i+1}) = (Q_\theta^{hi}(s_i, a_i) - R_i - \gamma Q_\theta^{hi}(s_{i+1}, \mu_\phi^{hi}(s_{i+1})))^2$, where a_i can be aw_i or aa_i . μ_ϕ^{hi} is trained to maximize $Q_\theta^{hi}(s_t, \mu_\phi^{hi}(s_i))$ over all s_i from the environment. μ_ϕ^{hi} is augmented with Gaussian noise. So actions are collected as $a_i \sim N(\mu_\phi^{hi}(s_i), \delta)$. During exploitation, δ is initialized to 0.5 and decayed after each episode exponentially. The LLC may be trained by simply incorporating g_t into the standard method, where g_t can be gw_t or ga_t . So the low-level Q-value function Q_θ^{lo} is to minimize the error $(Q_\theta^{lo}(s_i, g_t, a_i) - r(s_i, g_t, a_i, s_{i+1}) - \gamma Q_\theta^{lo}(s_{i+1}, g_t, \mu_\phi^{lo}(s_{i+1}, g_t)))^2$ for all transitions $(s_i, g_t, a_i, s_{i+1}, g_t)$. The policy μ_ϕ^{lo} is trained to maximize the Q-value $Q_\theta^{lo}(s_i, g_t, \mu_\phi^{lo}(s_i, g_t))$ for all sampled state-goal tuples (s_i, g_t) .

Correcting High level Training. AutoQB also corrects the high-level training [20, 21]. It takes high-level transition tuples $(s_{i:i+c-1}, g_t, a_{i:i+c-1}, R_{i:i+c-1}, s_{i+c})$, where $x_{i:i+c-1}$ denotes the sequence x_i, \dots, x_{i+c-1} collected by the HLC, and converts them to state-action-reward transitions $(s_i, g_t, \sum R_{i:i+c-1}, s_{i+c})$ which can be pushed into the replay buffer. However, since transitions obtained from past LLCs do not accurately reflect the actions that would occur if the same goal were used with the current LLC, AutoQB has to introduce a correction translating old transitions into ones that agree with the current LLC. AutoQB re-labels the high-level transition $(s_i, g_i, \sum R_{i:i+c-1}, s_{i+c})$ with a different high-level action \tilde{g}_t chosen to maximize the probability $\mu^{lo}(a_{i:i+c-1} | s_{i:i+c-1}, \tilde{g}_t)$. AutoQB computes 8 candidate goals sampled randomly from a Gaussian centered at G_t , the average QBN/BBN of the layer consisting of $OC_{i+c} \sim OC_i$. It also includes g_t and G_t . Among these 10 goals, AutoQB selects the minimal goal to re-label the experience.

$$\Omega(N) = 20 \log \left(\frac{a(N)^\alpha}{p(N)^\beta m(N)^\gamma} \right) \quad (2)$$

3.3. Search Protocols

Extrinsic Reward. After taking an action aw_i or aa_i at state s_i , AutoNB arrives at the next state s_{i+1} and receives an extrinsic reward R_i . The HLC aims to maximize the accumulative extrinsic reward $R = \sum \gamma^{i-1} R_i$, where $\gamma \in [0, 1)$ is a decay factor. As the immediate extrinsic reward, we adopt NetScore [35] shown in Equation 2, where $\Omega(N)$ is the NetScore for a network N ; $a(N)$ indicates inference accuracy; $p(N)$ means the sum of the QBN/BBN of each weight divided by 32 in the network; $m(N)$ indicates the number of logic operations (AND for quantization; XNOR for binarization) performed during an inference; and

α, β, γ are constant coefficients controlling the influence of accuracy, architectural complexity, and computational complexity of the network. By adjusting α, β, γ , AutoQB use various search protocols to explore the design space of network quantization/binarization for different scenarios on various hardware platforms. Through the Roofline model [34], AutoQB can balance the computing cost and memory accesses on a hardware platform by deciding β and γ . If the off-chip memory (on-chip computing power) is the bottleneck of a hardware system, AutoQB minimizes the BBN/QBN of network parameter (logic operation number) by increasing β (γ). For *resource-constrained* applications, e.g., drones, AutoQB set $\alpha = 1, \beta = 0$ and $\gamma = 0$ to achieve the best accuracy given the maximum amount of hardware resources. This reward offers no incentive for the reduction of architectural complexity or computational complexity, so AutoQB can reduce the QBN/BBN by limiting the action space. AutoQB allows arbitrary action at the first few layers and starts to limit the action when it find that the budget is insufficient even after using the smallest QBN/BBN for all the following layers. Algorithm 1 explains the process for action space limitation. For *accuracy-guaranteed* applications, e.g., fingerprint locks, AutoQB set $\alpha = 2, \beta = 0.5$ and $\gamma = 0.5$ to obtain the smallest computing overhead and model size with no accuracy loss.

Algorithm 1 A HLC predicts gw_t or ga_t for L_t in an m -layer network with the minimal allowed goal g_{min} , the average weight (activation) QBN/BBN, \overline{BBN}_w (\overline{BBN}_a).

```

1: %% Let  $g_t$  represents  $gw_t$  or  $ga_t$ .
2: procedure LAYERBOUND
3:   if  $t == 0$  then
4:     %% Initialize the XNOR # budget.
5:      $logic_{budg} = \sum_{i=0}^m logic_i \cdot \frac{\overline{BBN}_w}{32} \cdot \frac{\overline{BBN}_a}{32}$ 
6:     %% Initialize the actual XNOR #.
7:      $logic_{curr} = 0$ 
8:      $g_t = \mu^{hi}(s_t)$ 
9:     %% Compute the goal and bound it with  $g_{min}$ .
10:     $g_t = \max(g_t, g_{min})$ 
11:    %% Compute the XNOR # of following layers.
12:     $logic_{rest} = \sum_{i=t+1}^m logic_i$ 
13:    %% Compute the XNOR # must be reduced at
14:     $L_t$  if all the following layers are binarized with  $g_{min}$ .
15:     $logic_{duty} = logic_{budg} - (\frac{g_{min}}{32})^2 \cdot logic_{rest} - logic_{curr}$ 
16:    %% Bound  $g_t$  if it is too large to meet  $\overline{BBN}$ .
17:     $g_t = \min(g_t, (1 - \frac{logic_{duty}}{logic_t}) \cdot 32)$ 
18:    %% Update the actual XNOR #.
19:     $logic_{curr} = logic_{curr} + \frac{g_t}{32} \cdot logic_t$ 
20:  return  $g_t$ 

```

Intrinsic Reward. After the HLC generates a goal gw_t (ga_t), the LLC predicts an action aw_i (aa_i) through gw_t (ga_t) and state s_i . And then, the LLC arrives the next state s_{i+1} , receives an intrinsic reward r and maximizes the ac-

cumulative intrinsic reward $r = \sum \gamma^{i-1} r_i$. AutoQB adopts the shaped reward [4] as its intrinsic reward to take extrinsic reward into consideration and enable fine-grained low-level behavior learning. The intrinsic reward can be represented as $r_i = \zeta \cdot (-\|g_t \cdot N - \sum_{i=1}^N a_{t+i-1}\|_2) + (1 - \zeta) \cdot R_i$, where N is the output channel number in layer L_t ; R_i is the extrinsic reward; and ζ is a constant parameter defining the impact from the HLC. If $\zeta = 0$, the LLC strictly follows the order of the HLC. On the other hand, if $\zeta = 1$, the HLC has no direct influence on the LLC.

3.4. Storage Overhead

AutoQB uses 6-bit to store the QBN/BBN for a channel. The storage overhead of AutoQB is $< 0.3\%$ for various CNN models. For instance, ResNet-18 found by resource-constrained channel level AutoQB requires 8.3MB to store all quantized weight values in Table 2. *Res18-C* spends 9.31KB in recording all QBNs (each of which is $0 \sim 32$) of 5.8K weight output and 6.9K activation input channels.

4. Experimental Results

AutoQB uses a linear quantization strategy [38] to quantize a network and a simple binarization technique [17] to convert each input, weight and activation of a network to multi-bit binary codes $\{-1, +1\}$. The actors in AutoQB has two hidden layers, each with 300 units. The final output layer is a sigmoid layer producing an output scaled by 32. A goal is bounded to a floating point number within $[0, 32]$, while an action is bounded to an integer within $[0, 32]$. The critic of AutoQB also has two hidden layers, each of which consists of 300 units. AutoQB sets $\tau = 0.01$ for the soft target updates, and trains the network with the batch size of 64 and the replay buffer size of 2000. AutoQB first explores 100 episodes with a constant noise $\delta = 0.5$, and then exploits 300 episodes with exponentially decayed noise δ .

To evaluate our techniques, we selected several CNN models including CIFAR10-7CNN (**CIF10**), ResNet18 (**Res18**) and ResNet50 (**Res50**), SqueezeNetV1 (**SqNet**) and MobileNetV2 (**MoNet**). CIF10 includes 7 convolutional layers and is trained on the CIFAR10 database containing 50K training images spanning 10 categories of objects. AutoQB performs CIF10 inferences on 10K test images of CIFAR10. The other CNN models are trained on ImageNet including 1.26M training images and tested on 50K test images spanning 1K categories of objects. For all experiments, the accuracy in both extrinsic and intrinsic rewards is obtained on only validation images. The hierarchical DRL of AutoQB can finish searching on CIFAR10 within 1 hour on a GeForce GTX1080 GPU. But it takes $2 \sim 4$ days to search for a model on ImageNet on the same GPU.

4.1. Overall Performance

Network Quantization. We conducted both resource-constrained searches ($\alpha = 1, \beta = 0$ and $\gamma = 0$) and accuracy-guaranteed searches ($\alpha = 2, \beta = 0.5$ and $\gamma = 0.5$) on all models with their corresponding datasets by AutoQB.

Table 2: Network Quantization by AutoQB. $X-F$ indicates the full-precision model X . $X-N$ uses a QBN for the model X . $X-L$ assigns a QBN for each layer of the model X . And $X-C$ sets a QBN for each output channel of the model X .

Model	resource-constrained				accuracy-guaranteed			
	top-1 err (%)	top-5 err (%)	act QBN	wei QBN	top-1 err (%)	top-5 err (%)	act QBN	wei QBN
CIF10-F	6.22	0.22	-	-	6.22	0.22	-	-
CIF10-N	6.47	0.22	5	5	6.84	0.17	5	5
CIF10-L	6.23	0.22	4.34	5.47	6.84	0.18	3.23	3.16
CIF10-C	6.22	0.22	4.25	5.14	6.84	0.16	2.13	2.17
Res18-F	31.53	11.70	-	-	31.53	11.70	-	-
Res18-N	32.36	11.88	5	5	32.36	11.88	5	5
Res18-L	32.07	11.82	4.34	4.63	32.36	11.90	3.17	4.15
Res18-C	31.57	11.82	4.17	4.33	32.37	11.82	3.12	3.29
Res50-F	25.39	7.83	-	-	25.39	7.83	-	-
Res50-N	26.20	9.35	5	5	26.20	9.35	5	5
Res50-L	25.67	8.02	4.07	6.01	26.19	8.55	3.42	5.62
Res50-C	25.43	7.92	3.93	6.12	26.08	8.32	3.17	4.01
SqNet-F	43.28	20.87	-	-	43.28	20.87	-	-
SqNet-N	44.14	21.26	5	5	44.14	22.96	5	5
SqNet-L	43.67	21.14	4.56	5.27	44.03	22.74	4.12	4.28
SqNet-C	43.31	20.89	4.35	4.73	44.04	22.68	3.29	3.21
MoNet-F	28.37	9.08	-	-	28.37	9.08	-	-
MoNet-N	29.13	10.35	5	5	29.13	19.35	5	5
MoNet-L	28.78	9.57	4.61	5.12	29.13	19.35	4.12	3.97
MoNet-C	28.43	9.17	4.34	4.67	29.12	19.32	3.19	3.49

Table 3: Network Binarization by AutoQB.

Model	resource-constrained				accuracy-guaranteed			
	top-1 err (%)	top-5 err (%)	act BBN	wei BBN	top-1 err (%)	top-5 err (%)	act BBN	wei BBN
CIF10-F	6.22	0.22	-	-	6.22	0.22	-	-
CIF10-N	7.32	0.27	5	5	7.32	0.27	5	5
CIF10-L	7.02	0.22	4.59	4.27	7.22	0.22	4.17	4.36
CIF10-C	6.74	0.22	4.29	4.73	7.28	0.22	3.19	2.72
Res18-F	31.53	11.70	-	-	31.53	11.70	-	-
Res18-N	36.59	13.27	5	5	36.59	13.27	5	5
Res18-L	35.92	12.85	4.67	5.21	36.57	13.25	4.12	4.29
Res18-C	34.39	11.97	4.46	4.73	36.59	13.27	3.06	3.27
Res50-F	25.39	7.83	-	-	25.39	7.83	-	-
Res50-N	29.37	12.23	5	5	29.37	12.23	5	5
Res50-L	28.92	10.29	4.69	5.24	29.37	11.43	3.74	4.23
Res50-C	28.47	8.94	4.51	4.89	29.36	11.43	3.13	3.27
SqNet-F	43.28	20.87	-	-	43.28	20.87	-	-
SqNet-N	47.46	26.63	5	5	47.46	28.63	5	5
SqNet-L	46.92	25.2	5.17	4.62	47.39	28.61	4.57	4.12
SqNet-C	46.32	24.18	5.03	4.20	47.34	28.61	3.71	3.06
MoNet-F	28.37	9.08	-	-	28.37	9.08	-	-
MoNet-N	32.28	12.35	5	5	32.28	19.35	5	5
MoNet-L	32.19	11.27	4.66	5.28	32.27	19.35	4.27	3.92
MoNet-C	31.41	10.72	4.63	4.98	32.16	19.32	3.30	2.72

We compare AutoQB against the full precision models and the empirical quantization policy [16] in Table 2. The full precision models use 32-bit IEEE754 floating point formats. The empirical quantization policy uses 5-bit as the QBN to quantize the entire models. All data in Table 2 from finetuned models are reported as the average weight QBN of the network and the average activation QBN of the network. For resource-constrained searches, compared to full precision models, AutoQB degrades the inference accuracy by only $< 0.06\%$ when conducting channel level quantization, while the empirical quantization policy reduces the inference accuracy by $< 0.86\%$ with even higher computing costs. For example, *MoNet-C* requires 4.34-bit for activations and 4.67-bit for weights, so it spends only 81.1% of fixed point operations of the empirically quantized model in fin-

ishing the same task but with 0.06% higher top-1 accuracy. For accuracy-guaranteed searches, compared to resource-constrained searches, AutoQB has larger incentive to decrease the average QBNs for both activation and weights by 19.8% ~ 46.8%, but sacrifices the inference accuracy more significantly ($< 0.86\%$). Compared to deep CNN models, the accuracy-guaranteed searches introduce more significant accuracy degradation on compact models, e.g., *SqNet-C* and *MoNet-C*.

Network Binarization. AutoQB also binarizes all models by both resource-constrained searches and accuracy-guaranteed searches. The comparison between AutoQB, full precision models and results of an empirical binarization policy [17] is shown in Table 3. The original models rely on 32-bit floating point data representations. The empirical binarization policy has to use a 5-bit BBN to binarize the entire models. All results in Table 3 produced by fine-tuned models are presented as the average weight BBN of the network and the average activation BBN of a network. Compared to quantization, under the same computing cost budget, network binarization reduces the inference accuracy of all models more significantly. Even with larger BBNs for weights and activations, the binarized models found by AutoQB still cannot compete with the quantized models produced by AutoQB in terms of inference accuracy. For instance, in resource-constrained searches, binarized *MoNet-C* with $act_BBN = 4.63$ and $wei_BBN = 4.98$ decreases the inference accuracy by 3.04% over the original model, while quantized *MoNet-C* with $act_QBN = 4.34$ and $wei_QBN = 4.67$ sacrifices the inference accuracy by 0.06%. The comparison between resource-constrained and accuracy-guaranteed searches of network binarization follows the same trend as that of network quantization.

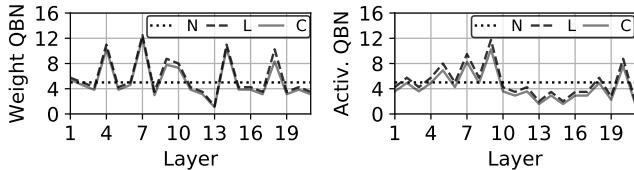


Figure 4: Average QBNs of Weights and Activations in each Layer of Res18 Made by Resource-Constrained Searches.

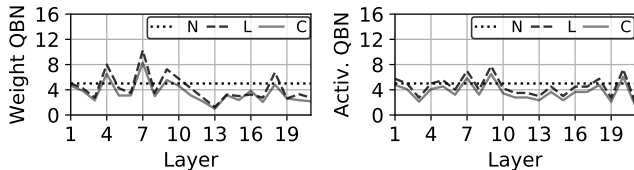


Figure 5: Average QBNs of Weights and Activations in each Layer of Res18 Made by Accuracy-Guaranteed Searches.

4.2. Output Channel Level Search

In this section, we highlight the output channel level exploration made by AutoQB. We provide more details and analysis on network quantization, since network binarization shares the same trend. The average QBNs of activations

and weights in each layer of *Res18* generated by resource-constrained searches are shown in Figure 4, while the ones made by accuracy-guaranteed searches are exhibited in Figure 5. The empirical quantization policy [17] only assigns one single QBN for all weights and activations of the entire network. On the contrary, AutoQB can automatically identify which layer or even which weight output (activation input) channel is more important and deserves a larger QBN. We show the average weight QBN distributions of layers 9 ~ 16 of *Res18* produced by output channel level AutoQB resource-constrained searches in Figure 6. Instead of offering each layer one QBN, AutoQB can predict a QBN for each weight output (activation input) channel in various layers and increases the inference accuracy by even less computing efforts.

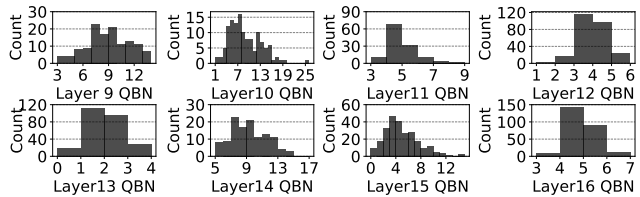


Figure 6: Weight QBN Distributions of Layers 9 ~ 16 of Res18 Generated by Output Channel Level Searches.

4.3. NetScore-based Extrinsic Reward

A recent DDPG-based AutoML network pruning framework [9] considers either the FLOP number ($F\#$) or the number of weights ($W\#$), but not both, in its reward. For network pruning, reducing $F\#$ is equivalent to decreasing $W\#$, since the channel pruning focuses on only weights. On the contrary, AutoQB has to take both weights and activations into consideration, so it adopts NetScore in its extrinsic reward to simultaneously balance the network inference accuracy, architectural complexity and computational complexity. The weight QBN reductions do not necessarily indicate the reductions on computational complexity, while decreasing the logic operation number may not necessarily reduce the weight QBNs. We used the FLOP-based extrinsic reward to limit only the logic operation number reduction and perform accuracy-guaranteed searches on *Res18*. We found a quantized *Res18* with roughly the same inference accuracy and approximately the same logic operation number as the one made by our accuracy-guaranteed AutoQB searches shown in Figure 5 (differences are $< 0.1\%$). The average weight and activation QBNs in each layer of *Res18* found with the FLOP-based reward are shown in Figure 7. Compared to its counterpart in Figure 5, the average weight QBN of the last fully-connected layer of *Res18* is larger, since the the FLOP-based reward does not have the motivation to reduce the number of weights in the last fully-connected layer.

4.4. Hierarchical Deep Reinforcement Learning

We evaluated and compare our hierarchical DRL-based AutoQB against a traditional DDPG-based AutoQB. The reward comparison during a resource-constrained output

channel level search on *CIF10* is shown in Figure 8. Hierarchical DRL-based AutoQB generates actions for all activation layers and weight channels in the network during one training episode. It gains $> 80\%$ inference accuracy after 200 training episodes. However, the traditional DDPG-based AutoQB is still stuck around 40% inference accuracy after 350 training episodes. The hierarchical DRL-based AutoQB significantly accelerates the design space exploration of network quantization and binarization by using both high-level goals and low-level actions.

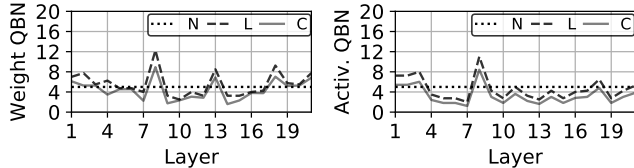


Figure 7: Average Weight and Activation QBNs in each Layer of *Res18* Found by the FLOP-based Reward [9].

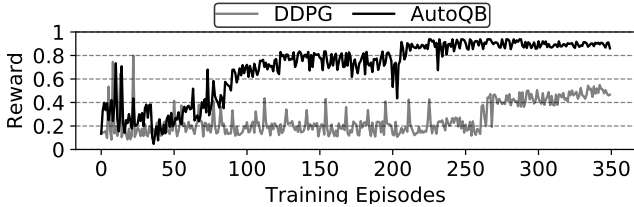


Figure 8: Average inference accuracy for 10 runs of AutoQB compared to DDPG.

4.5. Performance and Energy Analysis on FPGA

AutoQB can enable the fast and automatic design space exploration of network quantization on binarization trading-off the inference accuracy, computing overhead, and architectural complexity on a pre-trained model for mobile hardware developers. So the result of AutoQB, a quantized or binarized model, can be power-efficiently deployed on a mobile device often using embedded FPGAs [11, 22] to accelerate deep learning applications. We evaluated the performance and energy consumption of the models quantized and binarized by AutoQB by implementing the quantized [31] and binarized [30] CNN accelerator designs on a Xilinx Zynq-7000 ZC702 embedded FPGA. There are two types of accelerator architecture: *spatial* and *temporal* architectures. BitFusion [25] is a spatial CNN accelerator design deploying 2D systolic arrays of Fusion Units that spatially sum the shifted partial products of two-bit elements from weights and activations. In contrast, BISMO [31] is a temporal design of CNN accelerator using bit-serial multipliers. In each BISMO cycle, only 1-bit values from multiple weights and corresponding activations are multiplied, accumulated and shifted by bit-serial MAC units. Compared to the spatial design, the temporal architecture costs less FPGA resources and can be operated at higher frequency, since its communication cost is smaller and critical path is shorter. Moreover, the temporal architecture supports the quantized CNN models of AutoQB better, since the bit-serial multipli-

ers flexibly perform two operands with any QBNs without pipeline bubbles. In contrast, the spatial design can support only even-bit-width multiplications. So there are idle components in BitFusion units of the spatial architecture, when processing the quantized CNN models found by channel level AutoQB. We also created two kinds of binarized CNN FPGA-based accelerators by following both the temporal and spatial design styles.

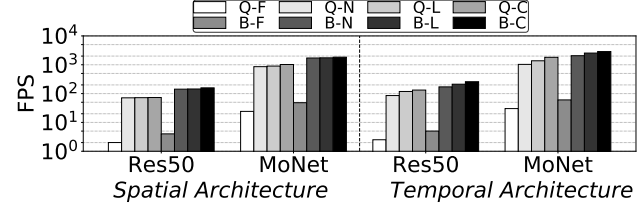


Figure 9: The performance comparison between quantized and binarized CNN models generated by resource-constrained searches of AutoQB. *Q* means quantization; *B* indicates binarization; *F* is the full-precision model; *N* uses a QBN/BBN for the model; *L* assigns a QBN/BBN for each layer of the model; *C* sets a QBN/BBN for each output channel of the model. The spatial architecture is operated at $100MHz$, while the temporal one works at $150MHz$.

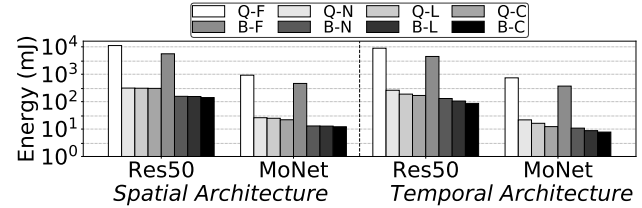


Figure 10: The energy comparison between quantized and binarized CNN models generated by resource-constrained searches of AutoQB.

Resource-Constrained Searches. The performance comparison between quantized and binarized *Res50* and *MoNet* generated by resource-constrained searches of AutoQB on spatial and temporal architectures is shown in Figure 9. The other CNN models share the same trend as *Res50* and *MoNet*. The performance results are reported as frames (images) per second (FPS). Through more fine-grained explorations, AutoQB decreases the average QBNs and BBNs for network quantization and binarization respectively. Therefore, for all models, setting a QBN/BBN to each output channel achieves better FPS over assigning a QBN/BBN to a layer or a network. Compared to quantization, network binarization improves the inference throughput by $58\% \sim 160\%$, due to its lower hardware cost (Figure 1(b)) for the same amount of convolutions in each output channel. Compared to the spatial architecture, the temporal implementation runs the channel level quantized/binarized models faster, because its sequential processing style can fully take advantage of the models assigning a QBN/BBN for each weight output and activation input channels. On the contrary, the spatial architecture suffers from pipeline bubbles when processing

channel level quantized/binarized models. The corresponding energy comparison is exhibited in Figure 10. Because of higher inference throughput, compared to quantized CNN models, their binarized counterparts decrease the inference energy by 37% ~ 54%. However, generally, as Table 2 and 3 illustrate, quantized CNN models obtain higher inference accuracy than binarized ones.

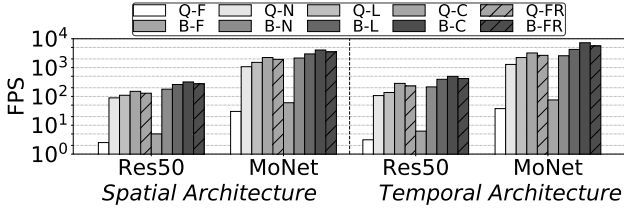


Figure 11: The performance comparison between quantized and binarized CNN models generated by accuracy-guaranteed searches of AutoQB. *FR* means the accuracy-guaranteed search by the Flop-based reward.

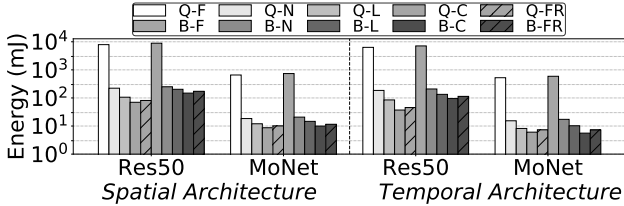


Figure 12: The energy comparison between quantized and binarized CNN models generated by accuracy-guaranteed searches of AutoQB.

Accuracy-Guaranteed Searches. The performance and energy comparisons between quantized and binarized *Res50* and *MoNet* generated by accuracy-guaranteed searches of AutoQB are shown in Figure 11 and Figure 12, respectively. Compared to the resource-constrained policy, the accuracy-guaranteed searches of AutoQB have stronger motivation to reduce the average QBNs and BBNs by degrading the inference accuracy more significantly. Therefore, compared to the quantized or binarized models found by resource-constrained searches, their accuracy-guaranteed search made counterparts increase the inference throughput by 75% ~ 186% on the FPGA, and decrease the inference energy by 8% ~ 91% on the FPGA. We also used the Flop-based reward [9] to conduct accuracy-guaranteed searches generating quantized and binarized CNN models whose performance and energy are also shown in the figures. Because of the limited off-chip memory bandwidth, the computing throughput of convolutional layers involving only a limited number of weights is much larger than that of fully-connected layers that have thousands of weights. A recent FPGA implementation [37] shows that for full-precision CNN models, the execution time of convolutional layers is approximately the same as that of fully-connected layers, because fully-connected layers spend a large portion of their execution time in fetching weights from off-chip main memories. Compared to

the Flop-based reward, our NetScore-based reward greatly decreases the weight number. Therefore, it improves the inference throughput by 29% and reduces the inference energy by 23% over quantized/binarized CNN models found by the Flop-based reward.

Table 4: Comparison against ReLeQ, AMC and HAQ.

Database	Model	Scheme	Top-1 Δ Acc	Top-5 Δ Acc	Norm. Logic
CIFAR-10	CIF10	ReLeQ [5]	-0.30%	-0.12%	15.6%
		AutoQB	-0.00%	-0.00%	3.15%
ImageNet	Res50	AMC [9]	-0.02%	0.03%	7.4%
		AutoQB	-0.01%	-0.02%	3.7%
	MoNet	HAQ [32]	-3.37%	-2.00%	1.6%
		AutoQB	-0.75%	-0.49%	1.4%

4.6. Comparisons against AMC, ReLeQ and HAQ

Prior works take advantage of DRL to prune [9] or quantize [5] a network. The deep RL-based AMC prunes 80% of weight output channels of ResNet-50 without inference accuracy degradation, so the overall computing cost of ResNet-50 is reduced to 7.4% of that of its full precision model. On the contrary, our accuracy-guaranteed AutoQB quantizes both activations and weights of ResNet-50 to averagely < 5-bit, thereby decreasing the computing cost of ResNet-50 to only 3.7%. ReLeQ employs LSTM-based RL to quantize only weights of a network. But due to the high complexity of LSTM, it can only quantize small models with small datasets, e.g., CIFAR-10. ReLeQ can only decrease the computing cost of a small CIFAR CNN to 15.6%. HAQ [32] uses DDPG to further decrease the speed of quantization design space exploration, but assigns two QBNs for weights and activations respectively in each layer. The layer level quantization of HAQ reduces the computing overhead of *MoNet* to 1.6%. In contrast, AutoQB uses hierarchical DRL to quantize both activations and weights of the same network at channel level. It greatly reduces the computing cost of the same CNN to only 1.4%. By even smaller computing costs, AutoQB still obtains higher inference accuracy than ReLeQ, AMC and HAQ.

5. Conclusion

Previous DRL-based network quantization frameworks [5, 32] support only coarse-grained layer level searches. It is still difficult for low power mobile devices, e.g., drones and VR computing systems, to deploy the quantized CNN models found by these DRL-based quantization frameworks, due to their limited battery lifetime. In this paper, we propose AutoQB for network quantization and binarization by leveraging hierarchical DRL to automatically search the channel level design space. AutoQB achieves fine-grained network quantization and binarization by searching a QBN or BNN for each weight output and activation input channels. With an universal extrinsic reward, AutoQB can perform various network quantization and binarization policies, e.g., resource-constrained and accuracy-guaranteed searches, by setting different parameters to the extrinsic reward.

References

- [1] A. Ashok, N. Rhinehart, F. Beainy, and K. M. Kitani. N2N learning: Network to network compression via policy gradient reinforcement learning. *CoRR*, abs/1709.06030, 2017. 2
- [2] B. Baker, O. Gupta, N. Naik, and R. Raskar. Designing neural network architectures using reinforcement learning. *CoRR*, abs/1611.02167, 2016. 2
- [3] M. Courbariaux, Y. Bengio, and J. David. Low precision arithmetic for deep learning. *CoRR*, abs/1412.7024, 2014. 1, 2
- [4] N. Dilokthanakul, C. Kaplanis, N. Pawlowski, and M. Shanahan. Feature control as intrinsic motivation for hierarchical reinforcement learning. *CoRR*, abs/1705.06769, 2017. 5
- [5] A. T. Elthakeb, P. Pilligundla, A. Yazdanbakhsh, S. Kinzer, and H. Esmaeilzadeh. Releq: A reinforcement learning approach for deep quantization of neural networks. *CoRR*, abs/1811.01704, 2018. 1, 2, 8
- [6] R. Gnanasekaran. A fast serial-parallel binary multiplier. *IEEE transactions on computers*, 10(8):741–744, 1985. 3
- [7] Y. Guo, A. Yao, H. Zhao, and Y. Chen. Network sketching: Exploiting binary structure in deep cnns. In *IEEE Conference on Computer Vision and Pattern Recognition*, pages 5955–5963, 2017. 2
- [8] S. Gupta, A. Agrawal, K. Gopalakrishnan, and P. Narayanan. Deep learning with limited numerical precision. In *International Conference on Machine Learning*, pages 1737–1746, 2015. 1
- [9] Y. He, J. Lin, Z. Liu, H. Wang, L.-J. Li, and S. Han. Amc: Automl for model compression and acceleration on mobile devices. In *European Conference on Computer Vision*, 2018. 1, 2, 3, 6, 7, 8
- [10] B. Jacob, S. Kligys, B. Chen, M. Zhu, M. Tang, A. Howard, H. Adam, and D. Kalenichenko. Quantization and training of neural networks for efficient integer-arithmetic-only inference. In *The IEEE Conference on Computer Vision and Pattern Recognition*, June 2018. 1
- [11] S. Jiang, D. He, C. Yang, C. Xu, G. Luo, Y. Chen, Y. Liu, and J. Jiang. Accelerating mobile applications at the network edge with software-programmable fpgas. In *IEEE Conference on Computer Communications INFOCOM*, pages 55–62, 2018. 7
- [12] K. Kandasamy, W. Neiswanger, J. Schneider, B. Póczos, and E. Xing. Neural architecture search with bayesian optimisation and optimal transport. *CoRR*, abs/1802.07191, 2018. 2
- [13] M. Kim and P. Smaragdus. Bitwise neural networks. In *ICML Workshop on Resource-Efficient Machine Learning*, 2016. 2
- [14] A. Krizhevsky, S. Ilya, and G. Hinton. Imagenet classification with deep convolutional neural networks. In *Advances in neural information processing systems*, 2012. 1
- [15] T. P. Lillicrap, J. J. Hunt, A. Pritzel, N. Heess, T. Erez, Y. Tassa, D. Silver, and D. Wierstra. Continuous control with deep reinforcement learning. In *International Conference on Learning Representations*, 2018. 1
- [16] D. Lin, S. Talathi, and S. Annapureddy. Fixed point quantization of deep convolutional networks. In *International Conference on Machine Learning*, 2016. 1, 2, 5
- [17] X. Lin, C. Zhao, and W. Pan. Towards accurate binary convolutional neural network. In I. Guyon, U. V. Luxburg, S. Bengio, H. Wallach, R. Fergus, S. Vishwanathan, and R. Garnett, editors, *Advances in Neural Information Processing Systems*, pages 345–353. Curran Associates, Inc., 2017. 1, 2, 3, 5, 6
- [18] J. L. McKinstry, S. K. Esser, R. Appuswamy, D. Bablani, J. V. Arthur, I. B. Yildiz, and D. S. Modha. Discovering low-precision networks close to full-precision networks for efficient embedded inference. *CoRR*, abs/1809.04191, 2018. 1
- [19] D. Miyashita, E. H. Lee, and B. Murmann. Convolutional neural networks using logarithmic data representation. *CoRR*, abs/1603.01025, 2016. 2
- [20] O. Nachum, S. Gu, H. Lee, and S. Levine. Data-efficient hierarchical reinforcement learning. In *Annual Conference on Neural Information Processing Systems*, 2018. 1, 2, 3, 4
- [21] O. Nachum, S. Gu, H. Lee, and S. Levine. Near-optimal representation learning for hierarchical reinforcement learning. In *International Conference on Learning Representations*, 2019. 1, 2, 3, 4
- [22] K. Ota, M. S. Dao, V. Mezaris, and F. G. B. D. Natale. Deep learning for mobile multimedia: A survey. *ACM Transaction on Multimedia Computing, Communications, and Applications*, 13(3s):34:1–34:22, June 2017. 7
- [23] R. Ramnarayanan, S. Mathew, V. Erraguntla, R. Krishnamurthy, and S. Gueron. A 2.1ghz 6.5mw 64-bit unified popcount/bitscan datapath unit for 65nm high-performance microprocessor execution cores. In *International Conference on VLSI Design*, pages 273–278, 2008. 2
- [24] M. Rastegari, V. Ordonez, J. Redmon, and A. Farhadi. Xnor-net: Imagenet classification using binary convolu-

- tional neural networks. In *IEEE European Conference on Computer Vision*, 2016. 2
- [25] H. Sharma, J. Park, N. Suda, L. Lai, B. Chau, V. Chandra, and H. Esmaeilzadeh. Bit fusion: Bit-level dynamically composable architecture for accelerating deep neural network. In *ACM/IEEE International Symposium on Computer Architecture*, pages 764–775, 2018. 7
- [26] K. O. Stanley and R. Miikkulainen. Evolving neural networks through augmenting topologies. *Journal Evolutionary Computation*, 10(2):99–127, June 2002. 2
- [27] L. Stewart and M. Stalzer. Bayesian optimization for parameter tuning of the xor neural network. *CoRR*, abs/1709.07842, 2018. 2
- [28] M. Sukanuma, S. Shirakawa, and T. Nagao. A genetic programming approach to designing convolutional neural network architectures. In *ACM Genetic and Evolutionary Computation Conference*, pages 497–504, 2017. 2
- [29] W. Tang, G. Hua, and L. Wang. How to train a compact binary neural network with high accuracy? In *AAAI Conference on Artificial Intelligence*, pages 2625–2631, 2017. 1, 2
- [30] Y. Umuroglu, N. J. Fraser, G. Gambardella, M. Blott, P. Leong, M. Jahre, and K. Visser. Finn: A framework for fast, scalable binarized neural network inference. In *ACM/SIGDA International Symposium on Field-Programmable Gate Arrays*, pages 65–74, 2017. 7
- [31] Y. Umuroglu, L. Rasnayake, and M. Sjalander. BISMO: A scalable bit-serial matrix multiplication overlay for reconfigurable computing. *CoRR*, abs/1806.08862, 2018. 7
- [32] K. Wang, Z. Liu, Y. Lin, J. Lin, and S. Han. HAQ: hardware-aware automated quantization. *CoRR*, abs/1811.08886, 2018. 1, 2, 3, 8
- [33] Y. Wang, C. Xu, J. Qiu, C. Xu, and D. Tao. Towards evolutionary compression. In *ACM SIGKDD International Conference on Knowledge Discovery & Data Mining*, pages 2476–2485, 2018. 2
- [34] S. Williams, A. Waterman, and D. Patterson. Roofline: an insightful visual performance model for multicore architectures. *Communications of the ACM*, 52(4):65–76, 2009. 3, 4
- [35] A. Wong. Netscore: Towards universal metrics for large-scale performance analysis of deep neural networks for practical usage. *CoRR*, abs/1806.05512, 2018. 3, 4
- [36] C. Xu, J. Yao, Z. Lin, W. Ou, Y. Cao, Z. Wang, and H. Zha. Alternating multi-bit quantization for recurrent neural networks. In *International Conference on Learning Representations*, 2018. 1, 2
- [37] C. Zhang, Z. Fang, P. Zhou, P. Pan, and J. Cong. Caffeine: Towards uniformed representation and acceleration for deep convolutional neural networks. In *IEEE/ACM International Conference on Computer-Aided Design*, pages 1–8, 2016. 8
- [38] A. Zhou, A. Yao, Y. Guo, L. Xu, and Y. Chen. Incremental network quantization: Towards lossless cnns with low-precision weights. In *International Conference on Learning Representations*, 2017. 1, 3, 5
- [39] S. Zhou, Z. Ni, X. Zhou, H. Wen, Y. Wu, and Y. Zou. Dorefa-net: Training low bitwidth convolutional neural networks with low bitwidth gradients. *CoRR*, abs/1606.06160, 2016. 2
- [40] B. Zoph, V. Vasudevan, J. Shlens, and Q. V. Le. Learning transferable architectures for scalable image recognition. *CoRR*, abs/1707.07012, 2017. 2